Safe Storage at Home: A Co-Simulation Approach for Short Circuit Current Characterisation

Daniel-Catalin Mitroi, Grigore Stamatescu
Automation and Industrial Informatics
University Politehnica of Bucharest
Bucharest, Romania
{daniel.mitroi1806, grigore.stamatescu}@upb.ro

Radu Plămănescu, Mihaela Albu
Faculty of Electrical Engineering
University Politehnica of Bucharest
Bucharest, Romania
{radu.plamanescu, mihaela.albu}@upb.ro

***Abstract*—Accurate real-time simulations contribute to the development of safe LVDC residential microgrid architectures and devices. In this context, the increased adoption of local home energy storage, as buffer between intermittent renewable, mostly solar pv, generation and typical energy usage profiles of residential consumers, can be driven by efficient fault protection methods. This increases trust in such solutions and enables the adoption of new current limiter (CL) devices that modulate the fault current with benefits for fast response time and seamless operation. CL design requires an efficient trade-off between material and device specifications and the operational use cases. For this reason, in this paper we discuss a co-simulation approach for deriving short circuit current curves by integrating MATLAB Simulink models with TyphoonHIL real-time emulation through the Functional Mockup Interface (FMI). Results from several scenarios based on parametrisation of key electrical components are presented and discussed. These lead to initial requirements for the design of new protection devices in LVDC microgrids.**

***Index Terms*—short circuit current, lvdc microgrids, co-simulation, real time, energy storage.**

I. Introduction

The increasing integration of renewable energy sources and the growing adoption of distributed energy resources have accelerated the development of low-voltage direct current (LVDC) systems and DC microgrids. Compared to traditional AC systems, LVDC networks offer improved efficiency, easier integration of storage systems, and enhanced controllability. However, protection in DC systems remains a major challenge due to the absence of natural current zero-crossing and the rapid rise of short-circuit currents.

One existing barrier in the implementation and wide spread adoption of low voltage direct current systems is represented by the development of new protection methods and tools, driven by improved understanding of failure modes and short circuit current characteristics in typical microgrid configurations [1], [2]. Reference models for short circuit currents are presented by [3] where a comparison is presented for average and passive models across various fault locations.

In this context, the EU-funded NOVETROL project aims to develop next-generation current-limiting (CL) devices based on high-mobility materials and the extraordinary magnetoresistance effect, and to integrate them into DC and hybrid AC/DC microgrids. It targets five application areas—DC loads, battery systems, photovoltaic systems, microgrids, and bidirectional EV supply equipment (EVSE) enabling vehicle-to-grid (V2G)—to support the European Green Deal by improving DC safety and reliability while reducing device cost, footprint, and environmental impact. These development areas have been mapped to detailed use cases and parametrised scenarios as follows [4]: *Cottage in the Sun (CoTS)*, focused on islanded PV installations, *Safe DC at Home*, focused on native and hybrid DC microgrids combining renewables, local storage and both DC and legacy AC devices, *Emerging DC at Work*, focused on higher powered industrial applications, and *DC in Motion*, for electric mobility applications.

Along with the above-mentioned use cases, the *Safe Storage at Home (SSH)* use case of NOVETROL, that is the objective of this paper, investigates the safe operation and graceful degradation of a residential energy storage system under short circuit fault conditions. This residential end-user setup comprises a Li-Ion battery interfaced to a common DC bus at V_{DC} through a bidirectional DC/DC converter that regulates the output voltage and operates in voltage-source mode for grid-forming-like behavior.

The main goal is to assess system resilience under a fault, i.e. short circuit, occurring on the link between the battery and the converter input. The analysed scenarios cover both normal and faulty conditions, considering operation without CL and potential CL operation for the particular short circuit profile.

Simulations are carried out using a co-simulation methodology that combines the software tools TyphoonHIL and MATLAB/Simulink to capture real-time dynamics and enable detailed and replicable fault studies as described in [5]. Multiple configurations are evaluated to quantify the impact of battery conditions such as state of charge (SOC), state of health (SOH), DC bus voltage levels e.g. 48 V, 220 V, 350 V, and converter limits on overall stability and safety.

Finally, the use case distinguishes between residential building-scale scenarios, which differ in demand profiles, current levels, and system sizing. The resulting insights inform the

This work has received funding from the European Union's Horizon Europe research and innovation programme under grant agreement No. 101192615 (NOVETROL).

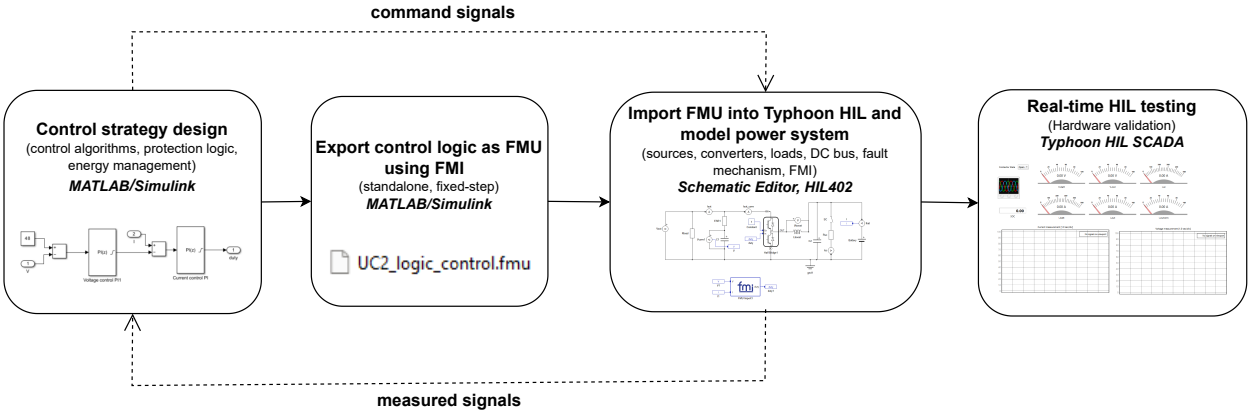

Fig. 1. Co-simulation workflow

optimisation of current-limiting strategies, improve resilience and fault tolerance in distributed energy systems, and clarify how battery chemistry and operating conditions influence protection approaches.

The main research objective and contribution of the work is thus aimed at the implementation and end-to-end validation of a co-simulation workflow for LVDC microgrids with residential storage modules for characterisation of short-circuit currents under several parametrisation and operation assumptions. This work contributes by validating a real-time co-simulation approach for LVDC fault studies, by providing comparative short-circuit characterization across different voltage levels and battery chemistries, and by extracting design-oriented insights relevant for current-limiting devices in the NOVETROL SSH use case.

The rest of the paper is structured as follows. Section II presents the implemented co-simulation methodology with references to relevant related work for defining the scientific context. Section III discusses the system implementation, including the control approach and battery models. Extensive case study results over multiple parametrisation scenarios are discussed in depth in Section IV. Section V concludes the paper with outlook on ongoing work.

II. Co-simulation Methodology within the State of the Art

The co-simulation approach for coupling complex system models using different tools is throroughly discussed by [6], including domain specific examples and theoretical fundamentals. [7] discussed a particular co-simulation approach for energy systems where the system model is implemented in specialized tools and the control algorithm runs in an open source Python-based environment with associated software libraries, while battery modelling co-simulation for converter design is introduced in [8]. A power hardware in the loop methodology is recently presented in [9], as relevant approach for industry-realistic applications.

The overall model was developed using a co-simulation architecture [10] that separates the power system model, implemented in Typhoon HIL, from the control strategy, which is designed in MATLAB/Simulink. The interface between the two environments is provided by exporting the control algorithms as a Functional Mock-up Unit (FMU), according to the FMI standard. This component is subsequently integrated into Typhoon HIL, where it interacts in real time with the electrical model by exchanging sampled values of the electrical voltage and current parameters of interest and the generated control command signals.

The resulting configuration allows real-time simulations and Hardware-in-the-Loop (HIL) tests via the SCADA interface, providing a robust framework for evaluating the performance, stability and robustness of control strategies in different operating scenarios. The diagram in Figure 1 illustrates the co-simulation framework that was designed and implementated.

The adopted methodology follows an integrated workflow structured into four main stages, transitioning from theoretical design to real-time validation. Initially, control algorithms, protection logic, and energy management strategies are developed in MATLAB/Simulink in discrete time. These are subsequently exported as an FMU, ensuring interoperability and deterministic execution in a tool-independent format suitable for closed-loop interaction.

In the implementation and testing phase, the FMU is integrated into the Typhoon HIL environment, where it operates in parallel with the detailed electrical model of the microgrid - comprising PV sources, storage systems, converters, and fault mechanisms - executed on FPGA-based hardware. The co-simulation framework enables bidirectional real-time signal exchange between the power model and the control logic, while monitoring and activation of short-circuit scenarios are performed through the SCADA interface. This hybrid approach ensures high fidelity and repeatability in characterizing fault currents, which is essential for optimizing protection devices in LVDC networks.

III. System Implementation

A. System Architecture

The TyphoonHIL power system model schematic implementation for the residential storage faults use case is shown in Figure 2. The diagram also illustrates the FMI/FMU interface that provides the linkage to the Simulink Simscape model providing the control commands. The short circuit fault location in this example is established at the battery terminals and can be triggered via software commands with nanosecond data logging and timestamp capabilities.

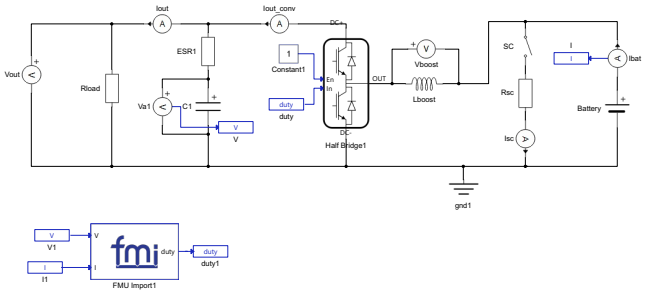

Fig. 2. TyphoonHIL Use Case Implementation Model

The modeled system consists of a battery energy storage unit connected to a DC busbar through a bidirectional DC–DC converter implemented as a half-bridge topology, enabling bidirectional power flow. The battery is modeled using both a user-defined approach and a Lithium-Ion electrochemical model, allowing the analysis of voltage dynamics as a function of the state of charge.

A short-circuit fault branch is introduced between the battery and the converter input, consisting of a controllable switch and a fault resistance, enabling controlled fault emulation and current measurement. The model also includes passive elements such as a battery-side capacitor and a transfer inductance, influencing transient behavior and current dynamics. On the DC bus side, a filtering branch and a resistive load are included, together with voltage and current measurement components, enabling detailed analysis of fault propagation and system response.

B. Control Strategy

The bidirectional DC-DC converter is regulated using a cascaded control structure with an outer voltage loop and an inner current loop. This grid-forming architecture separates fast and slow dynamics, ensuring stability and robustness under both normal and fault conditions.

The cascaded control structure is based on the principle of dynamic separation of time constants, according to which the current control loop is designed to exhibit significantly faster dynamics than the voltage control loop. Thus, the outer voltage loop considers the current subsystem as an almost ideal actuator, which simplifies controller design and improves the transient response of the system.

Figure 3 illustrates the general conceptual structure of the cascaded control strategy used for the bidirectional DC-DC converter, highlighting the external DC busbar voltage control loop and the internal battery current control loop.

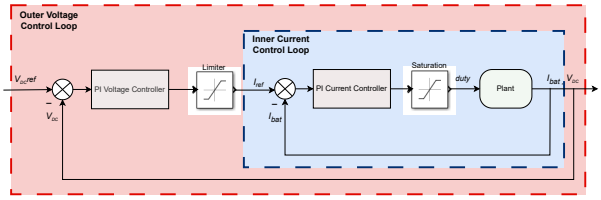

Fig. 3. Conceptual diagram of the cascaded control architecture

The outer control loop is responsible for maintaining the DC busbar voltage at the reference value $V_{\mathrm{DC,ref}}(t)$, corresponding to grid-forming operation of the storage system. The voltage error is defined as the difference between the reference and the measured value:

$$e_v(t) = V_{\mathrm{DC,ref}}(t) - V_{\mathrm{DC}}(t) \tag{1}$$

This error is processed by a PI controller, which generates the current reference for the inner loop: [11]

$$I_{\mathrm{ref}}(t) = K_{p,v} e_v(t) + K_{i,v} \int e_v(t)\, dt \tag{2}$$

The inner loop is responsible for fast regulation of the current through the bidirectional converter, ensuring the tracking of the reference I_{ref} and limiting electrical stresses on the power components. The current error is defined as:

$$e_i(t) = I_{\mathrm{ref}}(t) - I_{\mathrm{bat}}(t) \tag{3}$$

This error is processed by a second PI controller, which generates the converter control signal expressed as the duty cycle:

$$d(t) = K_{p,i} e_i(t) + K_{i,i} \int e_i(t)\, dt \tag{4}$$

C. Battery Modelling

The energy storage system is modeled using two complementary approaches available in the Typhoon HIL library, enabling both controlled parametric analysis and realistic representation of battery dynamics under fault conditions [12].

The first approach is based on a generic battery model described by a set of analytical equations, which capture the nonlinear voltage evolution as a function of the discharge state. This model is defined using three characteristic points on the battery discharge curve (Fig. 4): the fully charged state (V_{full}, Q), the end of the exponential zone $(V_{\mathrm{exp}}, Q_{\mathrm{exp}})$, and the end of the nominal zone $(V_{\mathrm{nom}}, Q_{\mathrm{nom}})$.

The battery is represented by a controlled voltage source E in series with an internal resistance R_{bat}. The voltage source is governed by the discharge state of the battery, defined as:

$$it = \int_0^t i_{\mathrm{bat}}\, dt \tag{5}$$

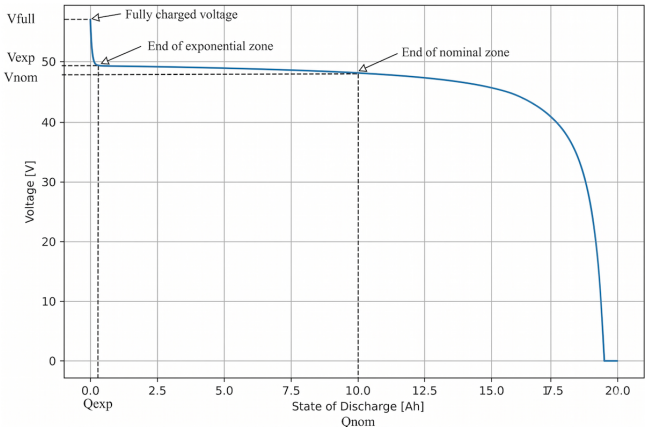

Fig. 4. Characteristic points of the user-defined battery discharge curve used in the LVDC simulations (based on TyphoonHIL)

The battery voltage is expressed as:

$$E = E_0 - K\,\frac{Q}{Q - it} + A\,e^{-it\,B} \tag{6}$$

where A represents the voltage drop in the exponential zone, B is the exponential zone factor, K is the polarization voltage, and E_0 is the voltage constant, defined as:

$$A = E_{\text{full}} - E_{\text{exp}} \tag{7}$$

$$B = \frac{3}{Q_{\text{exp}}} \tag{8}$$

$$K = \frac{\left(E_{\text{full}} - E_{\text{nom}} + A\left(e^{-B\,Q_{\text{nom}}} - 1\right)\right)(Q - Q_{\text{nom}})}{Q_{\text{nom}}} \tag{9}$$

$$E_0 = E_{\text{full}} + K + R_{\text{bat}}\,i - A \tag{10}$$

The internal resistance is computed assuming a battery efficiency of 99.5%:

$$R_{\text{bat}} = V_{\text{nom}}\,\frac{1 - 0.995}{0.2\,Q_{\text{nom}}} \tag{11}$$

Additionally, a user-defined battery model is employed, for explicit specification of the voltage–state of discharge relationship for controlled parametric studies. Furthermore, a LiIon electrochemical model is used, for detailed representation of nonlinear internal processes and enabling realistic simulation of battery behavior under severe conditions.

IV. Case Study and Simulation Results

A. Test Scenarios

Three representative test scenarios were considered, each corresponding to a different DC busbar voltage level (48 V, 220 V, and 350 V), while maintaining a maximum battery discharge current of 200 A.

These configurations reflect typical operating regimes of residential and LVDC microgrid applications, ranging from low-voltage systems with strict safety constraints to higher-voltage configurations associated with increased power transfer and system stress.

In all scenarios, the battery is connected to the DC busbar through a bidirectional DC–DC converter operating in grid-forming mode. A short-circuit fault is applied on the connection between the battery and the converter input, enabling the evaluation of system response under critical conditions. The system is initially operated in steady-state conditions before the fault is triggered, ensuring a consistent basis for comparison across scenarios.

Table I summarizes the analyzed configurations, including battery type, DC busbar voltage, and fault resistance values. Two battery models are considered in each case, enabling a comparative assessment of their influence on fault current dynamics.

TABLE I
Analyzed Simulation Scenarios

Scenario No.	Battery Type	Max battery discharge current [A]	DC busbar voltage (V_{DC}) [V]	R_{sc} [Ω]
1.1	User-defined	200	48	0.15
1.2	Lithium-Ion	200	48	0.18
2.1	User-defined	200	220	0.60
2.2	Lithium-Ion	200	220	0.80
3.1	User-defined	200	350	1.25
3.2	Lithium-Ion	200	350	1.35

B. Simulation Results

This section presents the results obtained from co-simulation using Typhoon HIL and MATLAB/Simulink for the three considered DC voltage levels. The analysis focuses on the system response under short-circuit conditions, with emphasis on fault current evolution, battery terminal voltage, DC busbar voltage, and the interaction between the control structure and the power stage.

For all scenarios, the fault is applied after the system reaches steady-state operation. The evaluation is based on monitoring key electrical quantities relevant for system safety and stress assessment, including battery current (I_{bat}), short-circuit current (I_{sc}), battery voltage, and DC busbar voltage (V_{out}).

Simulation parameters are adapted for each configuration, including the DC voltage reference in the control layer and the electrical parameters in the power model. These include battery characteristics, fault resistance, and load conditions, as summarized in Table II.

TABLE II
Simulation Parameters for the Analyzed Scenarios

Scenario no.	Battery type	V_{ref} [V]	V_{full} [V]	R_{bat} [Ω]*	R_{sc} [Ω]	R_{load} [Ω]
1.1	User-defined	48	118	0.1	0.15	10
1.2	Lithium-Ion	48	–	–	0.18	10
2.1	User-defined	220	118	0.5	0.60	210
2.2	Lithium-Ion	220	–	–	0.80	210
3.1	User-defined	350	118	0.8	1.25	530
3.2	Lithium-Ion	350	–	–	1.35	530

* Parameters specific to the User-defined model.

The results corresponding to the 48 V DC busbar configuration are presented in Fig. 5 and Fig. 6. In this low-voltage case, the system response is primarily influenced by

the current limitation imposed by the control structure and by the relatively low stored energy in passive components. All short circuit current figures list the time on the X-Axis, with a nanosecond (ns) timestep and current (A) or voltage (V) on the Y-Axis.

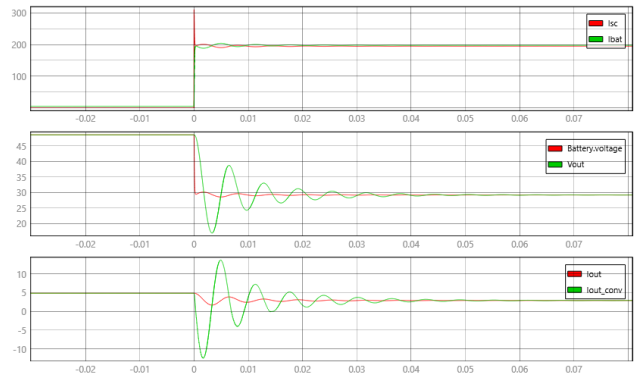

Fig. 5. Scenario 1.1 (V_{ref} = 48V, R_{sc} = 0.15 Ω)

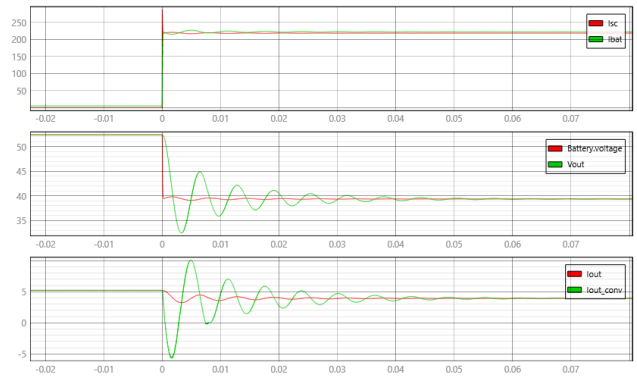

Fig. 6. Scenario 1.2 (V_{ref} = 48V, R_{sc} = 0.18 Ω)

Immediately after the short circuit application, the fault current ISC rapidly increases to values close to the maximum battery discharge current. Subsequently, the battery current Ibat stabilizes around the value enforced by the inner current control loop. The DC busbar voltage and battery voltage show a rapid decrease, accompanied by damped oscillations generated by the interaction between the transfer inductance, filtering capacitors, and PI controllers. It can be observed that the Lithium-Ion battery model exhibits a more robust response, characterized by improved damping and faster voltage stabilization compared to the user-defined model, which can be attributed to its more detailed electrochemical modelling.

For the scenarios operated at a DC busbar voltage of 220 V, the comparative results are shown in 7 and 8. The increase in voltage level leads to a significant amplification of the severity of fault-related transients. Although the maximum battery discharge current remains limited to 200 A by the control structure, the energy involved in the initial transient is considerably higher than in the 48 V case. In both battery models, a pronounced fault current peak is observed immediately after the short circuit initiation, followed by damped oscillations of current and voltage.

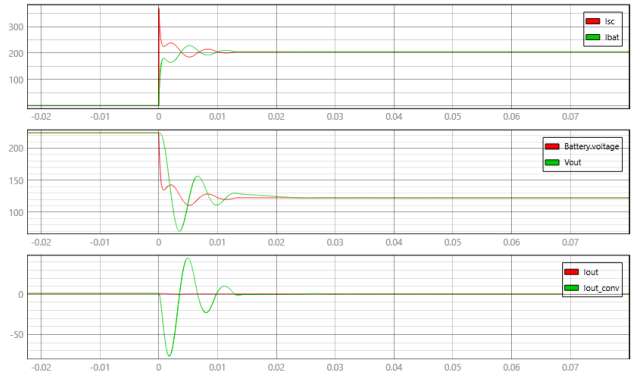

Fig. 7. Scenario 2.1 (V_{ref} = 220V, R_{sc} = 0.60 Ω)

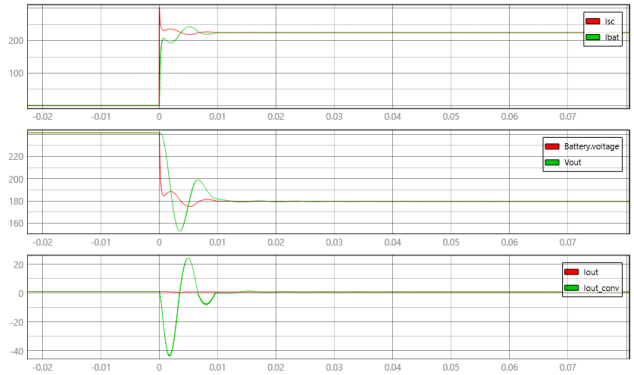

Fig. 8. Scenario 2.2 (V_{ref} = 220V, R_{sc} = 0.80 Ω)

The DC busbar voltage experiences a sharp drop and subsequently stabilizes at a value below the nominal level, indicating that the system has gone into a degraded operating mode. The differences between the two battery models became more evident in this configuration, with the Lithium-Ion model exhibiting better damped dynamics compared to the user-defined battery model.

The 350 V configuration (Fig. 9 and Fig. 10) represents the most severe operating condition. The high voltage level results in substantially increased electrical and energetic stress on system components, particularly during the transient phase immediately following fault occurrence.

The short circuit current quickly reaches high values, while the battery and DC busbar voltages undergo a sharp collapse, accompanied by large-amplitude oscillations. Although the inner current control loop effectively limits the current in steady state, the initial transient remains dominant and constitutes the primary risk factor for power electronic devices. Compared to the user-defined model, the Lithium-Ion battery exhibits faster voltage stabilization; however, the initial transient amplitude remains significant in both cases.

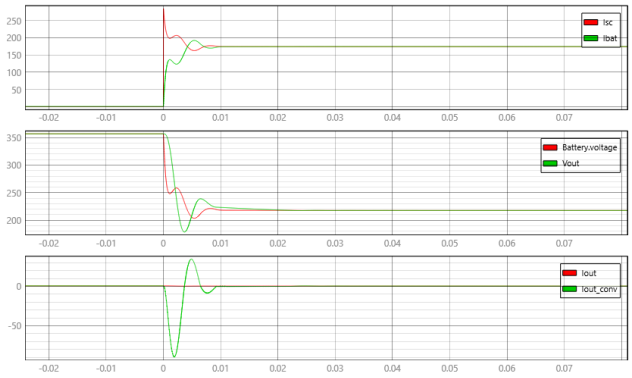

Fig. 9. Scenario 3.1 (V_{ref} = 350V, R_{sc} = 1.25 Ω)

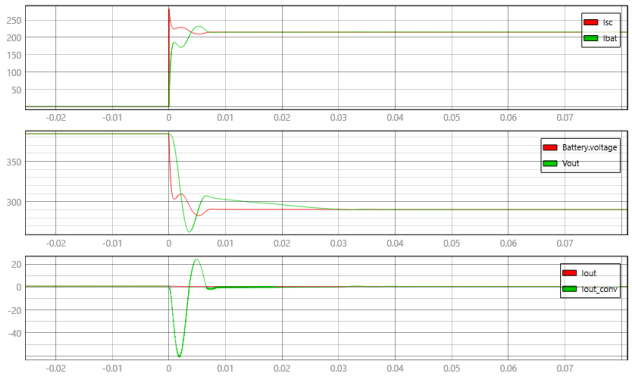

Fig. 10. Scenario 3.2 (V_{ref} = 350V, R_{sc} = 1.35 Ω)

The progression from 48 V to 350 V clearly highlights a gradual increase in fault severity as the DC busbar voltage level increases. While at 48 V the fault is characterized by limited currents and moderate transients, at 220 V and 350 V high-amplitude oscillations and significant stresses on the battery and DC-DC converter are observed.

V. Conclusions

This study demonstrates and validates a real-time co-simulation workflow for characterizing short-circuit currents in residential LVDC microgrids, using Typhoon HIL and MATLAB/Simulink integrated through the FMI standard. The approach ensures a safe, repeatable and high-fidelity environment for analyzing system resilience under various operating conditions and battery chemistries. The employed battery storage models enable a comparison of the influence of battery characteristics on short circuit current dynamics and DC voltage response. Results confirm a clear correlation between the DC bus voltage level and fault severity, with the 220 V and 350 V scenarios exhibiting substantially higher transient energy and stressing conditions compared to the 48 V configuration. Although the cascaded control strategy guarantees stable steady-state behavior, it is insufficient to mitigate the rapid current rise (di/dt) occurring in the first microseconds following a short circuit. Across all cases, the Lithium-Ion model proved more effective in capturing realistic transient dynamics than the user-defined model, highlighting the importance of accurate battery representation in LVDC protection studies.

These findings underline the need for ultra-fast and localized current-limiting (CL) solutions to ensure reliable protection of power electronic interfaces in residential microgrids. The practical insights extracted from the SSH use case contribute directly to the design requirements of next-generation CL devices foreseen within the NOVETROL project and beyond towards practical industrial applications.

Future work will extend the proposed framework to hybrid AC/DC topologies, investigate more complex microgrid configurations, and integrate prototype CL devices into real-time HIL validation scenarios using dedicated hardware-based emulation platforms.

References

[1] J. Gehring, R. Schwanninger, A. Nowak, B. Wunder, V. Lorentz, and M. März, "Method for detection and limitation of short-circuit currents for semiconductor circuit breakers in lvdc grids using a pre-saturated inductor," *IEEE Open Journal of Power Electronics*, vol. 6, pp. 524–536, 2025.

[2] J. J. Shea, T. Landry, and M. Liptak, "Short-circuit faults in dc microgrids," in *2024 IEEE Sixth International Conference on DC Microgrids (ICDCM)*, Aug. 2024, pp. 1–6.

[3] L. Bayerdörffer, T. Heurich, S. Rupp, S. Brüske, and M. Langwasser, "Simplified short circuit current simulation in lvdc microgrids," in *2025 IEEE Seventh International Conference on DC Microgrids (ICDCM)*, 6 2025, pp. 1–6.

[4] G. Stamatescu, M. Albu, M. Sanduleac, A. M. Dumitrescu, D. C. Mitroi, S. D. Costea, N. Fotias, S. Hesabirad, Y. Hazman, M. Gheamalinga, and R. Plamanescu, "D2.1 - Report on NOVETROL Use Cases and Scenarios," Zenodo, Report, Jun. 2025.

[5] D.-C. Mitroi, G. Stamatescu, R. Plamanescu, and M. Albu, "D2.2 – initial set of cl requirements formulated for each use case and scenario," Mar. 2026. [Online]. Available: https://doi.org/10.5281/zenodo.18923561

[6] C. Gomes, C. Thule, D. Broman, P. G. Larsen, and H. Vangheluwe, "Co-simulation: State of the art," *arXiv preprint arXiv:1702.00686*, 2017.

[7] D. L. Fernandes, A. L. M. Leopoldino, J. de Santiago, C. Verginis, A. A. Ferreira, and J. G. de Oliveira, "Distributed control on a multi-agent environment co-simulation for dc bus voltage control," *Electric Power Systems Research*, vol. 232, p. 110408, 2024.

[8] H. Li, W. Zhang, B. Sun, J. Jiang, Z. Yin, J. Wu, and X. He, "Lithium-ion battery modeling under high-frequency ripple current for co-simulation of high-power dc-dc converters," *Journal of Energy Storage*, vol. 54, p. 105284, 2022.

[9] G. De Carne, G. Lauss, S. D'Arco, S. Srdic, F. Wiegel, G. Buticchi, P. Kotsampopoulos, F. Ashrafidehkordi, F. Wald, K. Schoder, S. Hubschneider, A. Monti, A. Benigni, A. Paspatis, S. Cui, J.-J. Jung, M. Nazir, R. Cox, K. Strunz, V. Hagenmeyer, and J. Enslin, "Power hardware-in-the-loop for electrical systems: From research experience to guidelines for industrial testing," *IEEE Open Journal of Power Electronics*, vol. 7, pp. 822–842, 2026.

[10] D.-C. Mitroi, G. Stamatescu, R. Plamanescu, and M. Albu, "Co-simulation of shortcircuit current measurement in lvdc systems," in *2025 9th International Symposium on Electrical and Electronics Engineering (ISEEE)*. IEEE, 2025, pp. 1–6.

[11] C. Budai, T. Tóth-Katona, and P. Stumpf, "Novel design method for cascade control structure of electric drives: Closed-form expressions for control gains via pole placement," *IET Control Theory & Applications*, vol. 18, no. 17, pp. 2448–2467, 2024.

[12] *Typhoon HIL Documentation, Version 2026.1: Battery*, Typhoon HIL, 2026, available online. [Online]. Available: https://www.typhoon-hil.com/documentation/typhoon-hil-software-manual/References/battery.html